Optimized tower wall material, a numerical investigation on timber laminates

Master's thesis in Master Program Applied Mechanics (MPAME)

STEFAN ZORIC

DEPARTMENT OF INDUSTRIAL AND MATERIALS SCIENCE
CHALMERS UNIVERSITY OF TECHNOLOGY
Master's thesis IMSX30
Gothenburg, Sweden 2025

Master's thesis IMSX30

Optimized tower wall material, a numerical investigation on timber laminates

Final report

STEFAN ZORIC

CHALMERS
UNIVERSITY OF TECHNOLOGY

Department of Industrial and Materials Science
Division of Material and Computational Mechanics
Chalmers University of Technology
Gothenburg, Sweden 2025

Optimized tower wall material, a numerical investigation on timber laminates

STEFAN ZORIC

Supervisor: Tim Schüler, Uniso Technologies AB
Supervisor: Rode Löfgren, Modvion
Examiner: Prof. Leif Asp, Department of Industrial and Materials Science

Department of Industrial and Materials Science
Division of Material and Computational Mechanics
Chalmers University of Technology
SE-412 96 Gothenburg
Telephone +46 31 772 1000

Cover: Visualization of the maximum stress safety factor distribution in the wind turbine tower for a torsion-dominated load case.

Typeset in LaTeX
Printed by Chalmers Reproservice
Gothenburg, Sweden 2025

Optimized tower wall material, a numerical investigation on timber laminates
STEFAN ZORIC
Department of Industrial and Materials Science
Chalmers University of Technology

Abstract

Traditionally, wind turbine towers have been constructed using steel and concrete. However, growing environmental concerns, particularly the need to reduce carbon emissions, have caused the search for alternative solutions across various sectors, including wind energy. One such solution is the use of laminated veneer lumber (LVL) as a sustainable material for wind turbine towers. A notable example is the Wind of Change tower, developed by Modvion, which stands 105 meters tall and is built from spruce LVL panels assembled with adhesives. This innovative approach reduces the environmental impact associated with traditional materials like steel and concrete, while still ensuring that the tower meets structural performance requirements. However, the need to optimize the design to reduce material usage while maintaining performance still arises.

The aim of this thesis is to investigate whether an optimized tower design can achieve the same structural performance as existing solutions while minimizing material use. This is approached by designing two tower concepts and a benchmark model for a 166 meter tall wind turbine tower. Using Classic Laminate Theory (CLT), the study explores the effect of LVL panel orientations in different sections of the tower to identify an optimal orientation, referred to as the *sweet spot angle*, that maximizes safety factors under three defined load cases. The towers are evaluated against two failure criteria, Maximum Stress and Tsai-Hill, based on prior research correlating these criteria with the behavior of LVL wood. The investigation focuses solely on numerical simulations, with no experimental validation included in the scope. Results show that by optimizing the panel orientations, the total tower volume can be reduced by 15.4% while still meeting structural performance requirements.

Keywords: classic laminate theory, main grain direction, LVL panel, torsion, bending, failure criteria, maximum stress, tsai-hill, layup configuration.

Acknowledgements

Firstly I want to thank my supervisors Tim Schüler, Torkel Davidsson and Rode Löfgren for giving me the oppurtinity to do this project. Thank you for always being available to help whenever I had questions or concerns. You have taught me a lot of new things about the LVL industry, and how interesting it can be combining a well-known field with a less explored area. It has been a pleasure working with you at Modvion.

I would also like to thank my examiner Leif Asp for sharing his knowledge and great experience, providing me with valuable input throughout the project.

Finally, I want to thank all the incredible people and future colleagues I've met during my time at Chalmers. Every day brought a new lesson, and I have grown in all aspects of life. These moments are ones I will cherish for the rest of my life.

Stefan Zoric, Gothenburg, June 2025

List of Acronyms

Below is the list of acronyms that have been used throughout this thesis listed in alphabetical order:

ANSYS	Finite Element Analysis (FEA) software used for structural simulations
ACP (Pre, Post)	ANSYS Composite PrePost, add-on modules for defining and analyzing composite structures
DoP	Declaration of Performance
FEA	Finite Element Analysis
FEM	Finite Element Method
Kerto-Q	A brand of engineered LVL product, that belongs to the cross-banded category of LVL
Kerto-Qe	Modified version of Kerto-Q, developed and used by Modvion
LC1	First, bending-dominated, load case
LC2	Second, torsion-dominated load case
LC3	Third, general, load case
LVL	Laminated Veneer Lumber, engineered wood used in construction
LVL-C	Cross-banded LVL
LVL-P	Parallel LVL
TC1	Tower Concept 1
TC2	Tower Concept 2

Contents

List of Figures

List of Tables

1
Introduction

Traditionally, wind turbine towers are constructed using steel, a material known for its high strength, which is essential when constructing taller tower structures. The goal of reaching higher into the atmosphere to obtain greater and more stable wind speeds is enabled with the support of hybrid towers, typically combining concrete and steel. With this solution, a number of obstacles come along the way, such as significant carbon emissions and manufacturing difficulties [1]. As the push for sustainable energy grows, the focus is shifting toward alternative materials that align better with environmental goals. Wooden towers have emerged as a promising alternative. This innovative design aims to maintain the strength of traditional hybrid towers while significantly reducing environmental impact [2]. Wooden towers not only reduce the overall emissions, they also make transportation and assembly more efficient. In 2023, the first commercial wooden wind turbine tower, the Wind of Change, was built by Modvion, reaching a tower height of 105 m [3].

1.1 Aim

The aim of this project is to minimize the volume of the wooden tower by optimizing the laminate structure of the wall, using classic laminate theory. This is done for different load cases; one wind-dominated, one torsion-dominated and one balanced load case.

1.2 Limitations

This project has several limitations related to fixed parameters, scope of investigation, and methodological constraints. Firstly, certain key parameters are predefined and will not be optimized. These include the total height of the wind turbine tower, the applied loading conditions, and the LVL material properties, which are assumed to be constant throughout. Secondly, the investigation is performed at the panel level, where each LVL panel is treated as a single homogenoeus orthotropic unit. Finally, several aspects fall outside the scope of this project. The orientation and behavior of individual veneers within the LVL panels are not considered, even though they may influence the mechanical response. Furthermore, no physical testing is performed; all results are based on numerical simulations. Due to confidentiality agreements, exact values for loading conditions are not disclosed, thus reasonable approximations are used instead. Lastly, no buckling or frequency analysis will be performed.

2
Theory

The following chapter describes relevant theoretical aspects of the project. This includes principles related to laminated veneer lumber (LVL), the properties of cross-laminated configurations such as Kerto-Q and Kerto-Qe, and a summary of Classic Laminate Theory (CLT), which governs the mechanical behavior of layered composites. This chapter also covers relevant failure criteria used for analyzing and dimensioning the wall thickness of the tower.

2.1 LVL constructions

LVL is an engineered wood product that is made from logs by planing veneer sheets. Not only does the LVL-wood provide strength and durability to constructions, it also enables the use of wood that would otherwise go to waste [4]. The advantage of LVL used in timber construction is the high strength capacity of the structure, due to better material properties than sawn timber from the distribution and reduction of defects such as knots, which gives the possibility of reaching higher heights [2, 5]. There are two types of LVL-wood; Parallel LVL, referred to as LVL-P and Cross-banded LVL, also defined as LVL-C. The difference between the two lies in the orientation of the veneers. For LVL-P, all veneers are oriented in main grain direction (typically the longitudinal axis) with the aim to optimize for axial and bending strength in one direction. In the case of LVL-C panels, a small percentage of veneers are placed perpendicular to the main grain direction, which improves stability and stiffness across the grain, while keeping most strength in the primary direction [4, 6]. Figure 2.1 shows the material orientations used for the LVL [7].

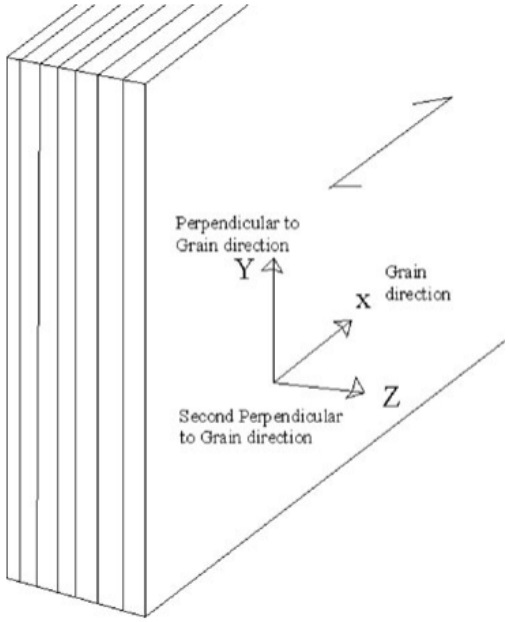

Figure 2.1: Conventional coordinate directions for LVL, showing grain (X), transverse (Y), and through-thickness (Z) orientations.

2.1.1 Kerto-Q and Kerto-Qe

LVL Kerto-Q is a spruce plywood constructed by Metsä Wood which belongs to the cross-banded category of LVL panels. It is produced of 3 mm thick veneers glued together to form a continuous sheet. These panels consist of approximately 10 – 20% of cross-banded veneers [8]. The thicknesses presented in Table 2.1 represent standard configurations for LVL-C panels. However, in this study, the following thicknesses were used: 16 mm, 19 mm, 22 mm, 25 mm, 28 mm, and 31 mm. This adjustment is due to Modvion's manufacturing process, where the faces of the panels are ground by 1 mm on each side to improve the adhesion of the glue.

Table 2.1: Layup configurations and characteristics of LVL-C panels.

Thickness [mm]	Number of veneers	Layup of LVL-C	Number of cross-veneers
18	6	||–||	2
21	7	||-|-||	2
24	8	||-||-||	2
27	9	||-|||-||	2
30	10	||-||||-||	2
33	11	||-|||||-||	2

In this report LVL Kerto-Qe will also be mentioned, which is a modified version of Kerto-Q, developed and used by Modvion. The material properties slightly differ between the two and are used for different purposes in this study. In Table 2.2, the material properties for the two LVL types used throughout the project are listed.

Table 2.2: Material properties used for simulations throughout this project.

Property		Symbol	Unit	Kerto-Q	Kerto-Qe
Tension strength	∥ grain	$\sigma_{x,t}$	[MPa]	22	28
	Edgewise, ⊥ grain	$\sigma_{y,t}$	[MPa]	5	6
	Flatwise, ⊥ grain	$\sigma_{z,t}$	[MPa]	0.1	0.5
Compression strength	∥ grain	$\sigma_{x,c}$	[MPa]	26	28
	Edgewise, ⊥ grain	$\sigma_{y,c}$	[MPa]	9	6
	Flatwise, ⊥ grain	$\sigma_{z,c}$	[MPa]	2.2	2.2
Shear strength	Edgewise, ∥ grain	τ_{xy}	[MPa]	4.5	4.6
	Flatwise, ∥ grain	τ_{xz}	[MPa]	1.3	1.3
	Flatwise, ⊥ grain	τ_{yz}	[MPa]	0.6	0.6
Modulus of elasticity	Longitudinal (l)	E_x	[MPa]	10500	12000
	Tangential (t)	E_y	[MPa]	2000	1845
	Radial (r)	E_z	[MPa]	130	130
Shear modulus		G_{xy}	[MPa]	600	510
		G_{xz}	[MPa]	120	120
		G_{yz}	[MPa]	22	22
Poisson's ratio	lt	ν_{xy}	[–]	0.1	0.11
	tr	ν_{yz}	[–]	0.7	0.7
	lr	ν_{xz}	[–]	0.8	0.81
Density		ρ_{mean}	[kg/m^3]	600	600

2.2 Classic Laminate Theory

Laminated composites are formed by bonding two or more laminae on top of each other. In this study, one LVL panel (consisting of a certain number of veneers) will be considered as one lamina. Each lamina can have its own rotation which contributes to increased stiffness and strength in a laminate. In *classic laminate theory* (CLT), the bond between laminae is assumed perfect. It is infinitesimally thin and not shear deformable so that laminae do not slip over each other and displacements remain continuous across the bond. This assumption allows all displacements at any point in the laminate to be related to the geometric mid-plane of the laminate [9]. Worth noting is that the disadvantage with the assumption made in CLT is that it does not cover the possibility of delamination of the laminae [10].

The laminate constitutive relations relate applied forces and moments to the laminate mid-plane strains and plate curvatures by following equation:

$$\begin{Bmatrix} N_x \\ N_y \\ N_{xy} \\ M_x \\ M_y \\ M_{xy} \end{Bmatrix} = \begin{bmatrix} A_{11} & A_{12} & A_{16} & B_{11} & B_{12} & B_{16} \\ A_{12} & A_{22} & A_{26} & B_{12} & B_{22} & B_{26} \\ A_{16} & A_{26} & A_{66} & B_{16} & B_{26} & B_{66} \\ B_{11} & B_{12} & B_{16} & D_{11} & D_{12} & D_{16} \\ B_{12} & B_{22} & B_{26} & D_{12} & D_{22} & D_{26} \\ B_{16} & B_{26} & B_{66} & D_{16} & D_{26} & D_{66} \end{bmatrix} \begin{Bmatrix} \epsilon_x^0 \\ \epsilon_y^0 \\ \gamma_{xy}^0 \\ \kappa_x \\ \kappa_y \\ \kappa_{xy} \end{Bmatrix} \tag{2.1}$$

where the matrices A, B, and D are called the *extensional stiffness matrix*, *coupling stiffness matrix*, and *bending stiffness matrix*, respectively. The A-matrix relates the resultant forces to the mid-plane strains, while the D-matrix relates the resultant moments to the plate curvatures. The values of A_{16} and A_{26} (marked with red) being zero indicate the absence of extension-shear coupling. This condition is achieved by using a balanced, unidirectional, or cross-ply stacking sequence. For symmetric laminates the values $B_{ij} = 0$, meaning that the coupling between bending and extension does not exist. The widespread use of symmetric laminates is primarily due to their ability to maintain structural and dimensional stability. Values of D_{16} and D_{26} are indicators of bending-twisting coupling in a laminate. Setting these terms to zero requires a balanced stacking sequence: for every $+\theta$ ply above the laminate mid-plane, there must be a corresponding $-\theta$ ply of equal material properties and thickness placed symmetrically below [9, 10].

2.2.1 Different orientation for different purposes

There are *laminate stacking sequences* (LSS) that are more common than others. Different sequences are used for different purposes. The stacking sequence, defined by the number of plies, their orientation angles, thicknesses, and material types, has a significant influence on the overall performance of the composite laminate. The most common sequence is the unidirectional laminate where all the laminas have the same orientation angle, typically 0°, to sustain axial and bending loads. Another common stackup sequence is the symmetric laminate, where the layup configuration is mirrored about the mid-plane of the laminate. Symmetry helps eliminate bending-extension coupling. Balanced laminates are also frequently used, eliminating in-plane shear coupling. Finally, a particularly useful variant is the angle-ply laminate, which consists solely of rotated plies. These are especially effective for handling torsional loads [10]. Understanding these standard stacking sequences is essential to interpreting the structural behavior of composite components in this study.

The layup configuration is written as a sequence of ply orientation angles enclosed in brackets, for example:

$$[\theta_1/\theta_2/\ldots]_S,$$

where each θ_i denotes the ply orientation angle relative to a reference direction. The subscript S indicates that the stacking sequence is symmetric about the mid-plane of the laminate. Symmetry can be either even or odd. Even symmetry means the entire stacking sequence, including the middle ply, is mirrored about the mid-plane.

This is written without a bar on the middle ply orientation. For example, the layup

$$[0°/45°/-45°]_S$$

expands to

$$[0°/45°/-45°/-45°/45°/0°],$$

where the full sequence is mirrored evenly. Odd symmetry means that the last ply in the sequence acts like the mid-plane, and the stacking is mirrored about that ply. This is indicated by a bar on the last ply angle in the notation. For example,

$$[0°/45°/\overline{90°}]_S$$

represents a layup where all plies except for the middle ply oriented at 90° are mirrored, which expands to

$$[0°/45°/90°/45°/0°],$$

resulting in an odd number of plies.

2.2.2 Thickness calculations

Analytically, the required thickness for certain panel orientations can be dimensioned by accounting for maximum stress during tosional and axial loads [9]. The computation of the maximum torsional shear stress in a thin-walled tube constructed from balanced symmetric laminates is expressed as follows:

$$\tau_{xy} = \frac{T}{2\pi \cdot (\frac{D}{2})^2 \cdot t_{45}}, \tag{2.2}$$

where T represents the applied torsional load, D is the diameter of the tube (in this case the tower) and t_{45} is the thickness of the ±45° panel. From this expression, the requried thickness for twisted panel at a ±45° angle, can be calculated for a given torsional load. This approach helps getting hand on what thickness is approximately needed to withstand a particular applied load.

To calculate the total thickness of the LVL panels with an orientation angle of 0°, the reaction forces in the tower are studied instead. The thickness for those panels can be dimensioned so that it can prevent crushing. The reaction force along the height of the tower, in the longitudinal direction, is essential. This force can then be used to decide the total thickness needed for the 0°-panels to avoid crushing:

$$\sigma_{x,c} = \frac{F_r}{\pi \cdot ((\frac{D}{2})^2 - (\frac{D}{2} - t_{0,crushing})^2)}, \tag{2.3}$$

where $\sigma_{x,c}$ is the compressive strength limit in the longitudinal direction, F_r is the reaction force, and $t_{0,crushing}$ is the total required thickness for 0° panels.

2.3 Failure criteria

A failure criterion is used to predict the strength condition for a material by interpreting cases of combined loads from a small number of material parameters. Different materials exhibit different responses to stress — for instance, isotropic materials behave the same in all directions, while orthotropic or anisotropic materials (such as composites and wood-based products like LVL) have direction-dependent properties. Thus, no single failure criterion is universally applicable, and multiple criteria are often compared for a specific application [11]. In this study, two stress-based failure criteria are selected: Maximum stress and Tsai–Hill, due to the fact that they only require tensile, compressive, and shear strength values. A previous study evaluated the performance of various failure criteria in predicting the strength of LVL made from radiata pine veneers under off-axis loading, i.e. loading applied at an angle to the main grain direction. The study found that the correlation between predicted and experimental strength varied with grain angle. The **Maximum stress** criterion showed good agreement for grain angles above 45°, but less accurate predictions for smaller angles. The **Tsai–Hill** criterion generally underestimated the strength at grain angles between 15° and 45°, with the largest deviation at 15° [12].

Table 2.3: Comparison between measured and predicted tensile strength of LVL for different grain angles.

Strength (N/mm^2)	**Grain angle** (°)				
	0	**15**	**30**	**45**	**90**
Measured					
	5.18	1.22	0.50	0.32	0.18
Predicted					
Maximum stress	5.18	0.72	0.42	0.36	0.18
Tsai-Hill	5.18	0.69	0.36	0.25	0.18

The values in Table 2.3 indicate that while both criteria can be used for general estimations, they may be less reliable for cases with small deviations from the grain direction. Similarly, other research on plywood confirmed that the maximum stress criterion yielded the closest match to measured values. Notably, all criteria tended to underestimate the strength, indicating conservative predictions [13].

2.3.1 Maxmimum stress and Tsai-Hill

The Maximum stress criterion assumes that failure occurs when any individual stress component exceeds its corresponding strength limit, either in tension or in compression. It treats each stress mode (longitudinal, transverse, shear) independently and does not account for interaction between stress components [10, 13].

$$\left(\left|\frac{\sigma_x}{X}\right|, \left|\frac{\sigma_y}{Y}\right|, \left|\frac{\tau_{xy}}{S}\right|\right) = 1 \tag{2.4}$$

The Tsai–Hill Criterion is a failure theory developed for anisotropic materials like composites. It considers interaction between stress components, making it more

conservative than the maximum stress approach. However, one limitation is that it does not differentiate tensile and compressive strengths, which can lead to inaccurate predictions for materials with asymmetric behavior [13].

$$\left(\frac{\sigma_x}{X}\right)^2 + \left(\frac{\sigma_y}{Y}\right)^2 + \left(\frac{\tau_{xy}}{S}\right)^2 - \frac{\sigma_x \sigma_y}{X^2} = 1 \tag{2.5}$$

For both Eqs. 2.4 and 2.5, X, Y and S denote the allowable strength of the panel in the longitudnal main grain direction (0°), transversal direction (90°) and in-plane shear strength between the longitudinal and transversal direction, respectively. The actual longitudinal, transverse and shear stress in the panel are represented by σ_x, σ_y and τ_{xy}.

3
Method

This chapter provides a detailed description of the method used in this project, including the implementation in ANSYS, hand calculations and laminate modelling. Additionally, an overview of how the data was analyzed is explained.

3.1 ANSYS implementation

The FEA software used for numerical investigation was ANSYS. In this section the ANSYS interface, seen in Figure 3.1, will be explained how it was constructed and modeled.

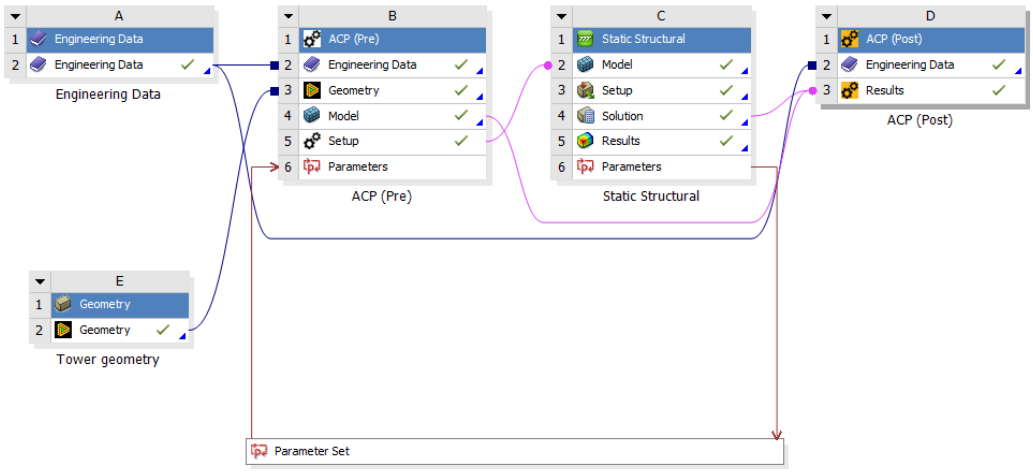

Figure 3.1: Representation of the workflow in ANSYS.

Relevant add-on modules and systems for this type of problem are the ACP Pre and ACP Post modules, as well as the Static Structural system. The connection between the ACP Pre setup and the model was established through a transfer shell composite data linkage.

3.2 FE Model preparation

The initial tower design was created as a shell model, which is preferred for cases with thin-walled structures where laminates are examined. The dimensions of the tower are shown in Figure 3.2.

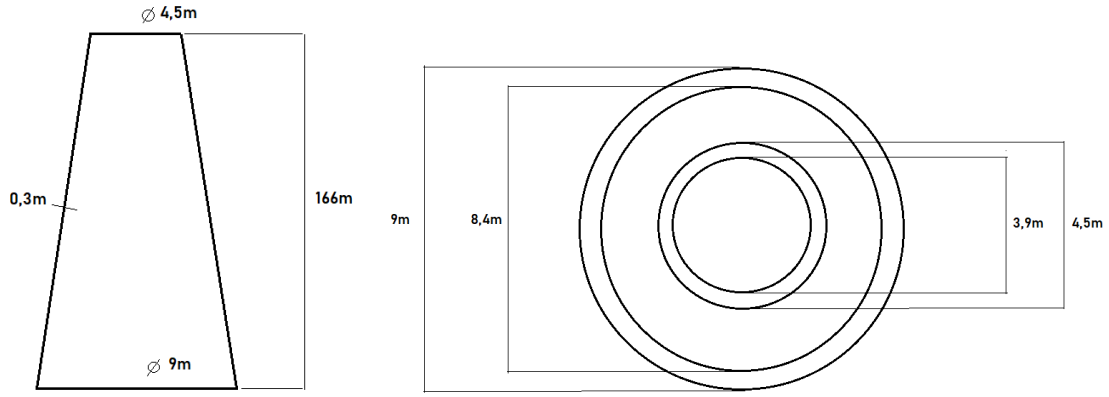

(a) Front view **(b)** Top view

Figure 3.2: Illustration of the tower geometry.

Initially, the thickness of the tower wall was set to 300 mm which equals to 12 LVL panels with a thickness of 25 mm each. This value served only as a preliminary input for the modeling process. The composite layup representing the laminated wall structure was defined using the ACP Pre & Post modules. The tower was meshed with an element size of 0.4 m. The top and bottom of the tower are connected to other components via steel joints, which are significantly stiffer than the LVL structure. To prevent boundary condition singularities and ensure that local stress concentrations near the rigid connections do not influence the results, the outermost row of mesh elements was disregarded at both ends. Additionally, a deformable load application behavior was used, allowing for ovalization of the tower edge under load. This is especially important at the top, where ovalization can lead to increased local stresses. By allowing this deformable behavior, the model reflects a worst-case scenario, leading to a more conservative design.

3.3 Tower Concepts

Two tower concepts were studied in this project. The first concept, referred to as **TC1**, was based on standard LVL Kerto-Q properties. This allowed full flexibility in design: the panel orientations were freely chosen, and the panel thicknesses were adjusted in small increments (3 mm), as described in chapter 2.1.1, enabling detailed layup optimization. The second concept, **TC2**, was based on Modvion's modified LVL Kerto-Qe data. This material configuration places stricter constraints: panel orientations were limited to $\pm 25°$, to ensure manufacturability and formability given the current production methods and structural demands. Furthermore, only one fixed panel thickness (25 mm) was available, which meant that changes in wall thickness could only be made in discrete steps by adding or removing entire panels. This resulted in a more constrained and structurally demanding design process.

To evaluate the effectiveness of the optimized tower concepts, a **benchmark model** was introduced. This reference configuration used only 0°-oriented panels along the entire tower and followed the same material (Kerto-Qe) and panel thickness (25

mm) constraints as TC2. It also reflects the simplest and most practical design to manufacture. The benchmark served as a baseline for comparison of the material usage, where total tower volume (volume of solid wood) was used as the primary parameter.

3.4 Boundary- and load conditions

The only boundary condition needed was a fixed support at the base of the tower, restricting all degrees of freedom. The tower is exposed to four different loads: the weight from the turbine, the horizontal wind force, and the torsional and bending moments form the turbine. Additionally, the self-weight of the structure is included in the calculations. In Figure 3.3 the three load conditions are illustrated.

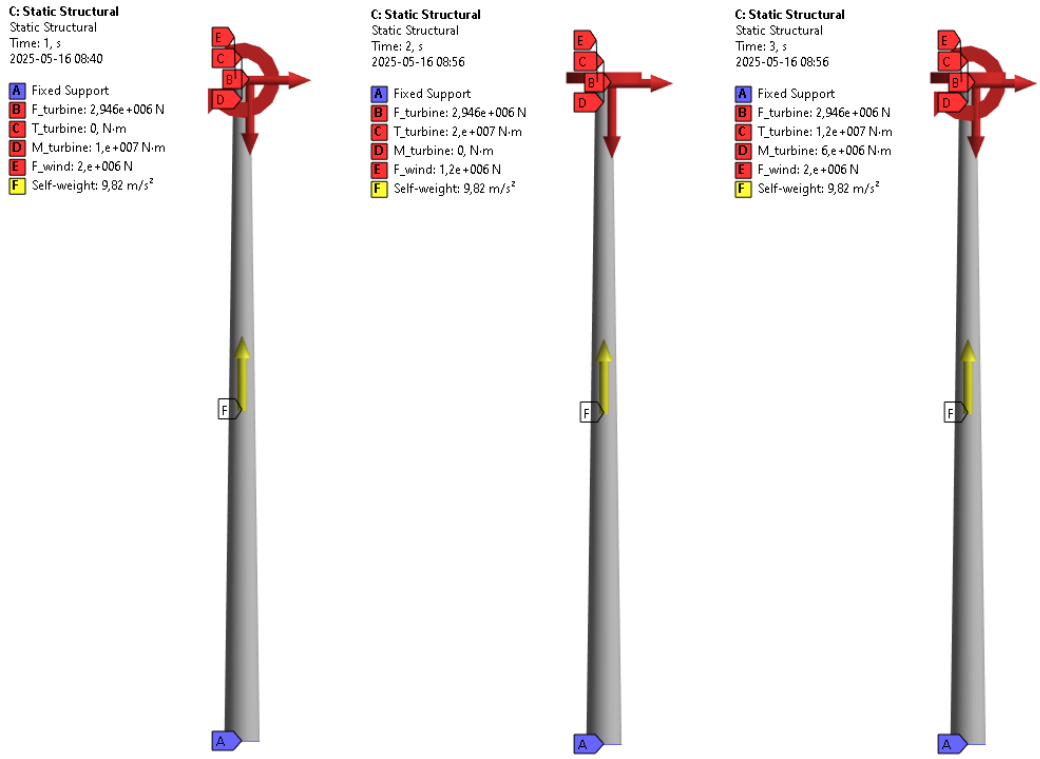

(a) LC1 **(b)** LC2 **(c)** LC3

Figure 3.3: Visualization of the applied loads on the tower in ANSYS, including force and moment directions along with their respective magnitudes.

Since the probability of all maximum loads occuring simultaneously is minimal, the loading conditions were divided into three load cases to represent more realistic scenarios. One load case is dominated by wind loads (LC1), another by torsional effects (LC2), and the third represents a more balanced distribution of forces (LC3). The three load cases used in this study are presented in Table 3.1.

Table 3.1: Load cases for the tower design

Load	LC1	LC2	LC3
F_{tower} **(Self-weight)**	✓	✓	✓
F_{turbine} **(300 tonne)**	✓	✓	✓
F_{wind} **(2000 kN)**	**(full)**	**(reduced)**	**(full)**
T_{turbine} **(20,000 kNm)**	✗	**(full)**	**(reduced)**
M_{turbine} **(10,000 kNm)**	**(full)**	✗	**(reduced)**

It is worth noting that the weight of the turbine and the self-weight of the tower remain the same for all three load cases, commonly referred to as **Dead loads**. In contrast, the remaining loads can vary and therefore do not reach their absolute maximum simultaneously. These are known as **Environmental loads**. The reduced forces in Table 3.1 are adjusted using the *Psi factor* (Ψ) according to the Ultimate Limit State (ULS) load combination rules in Eurocode 1 (EN 1990, Table A1.1) [14]. Specifically, the reduction factor for wind loads is $\Psi_{0,wind} = 0.6$.

3.5 Tower divided into sections

While the external loads themselves (axial, bending, torsional) are applied at the top of the tower, the internal stress distribution changes along its height. This implies that different layup configurations will allow better material utilization. As a consequence, the tower was divided into nine sections along its height, see Figure 3.4.

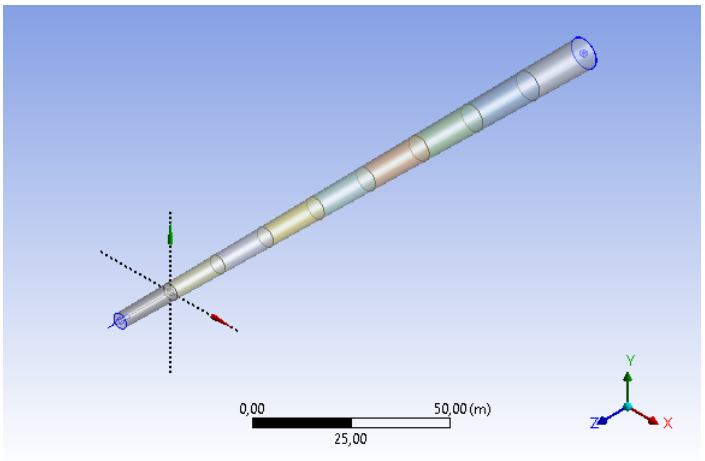

Figure 3.4: Visualisation of the divided tower geometry in nine sections.

The decision to divide the tower into nine sections was based on transportation and manufacturing constraints. According to Modvion's current practices, no section should exceed 20 m, which gives a minimum of nine sections needed in the tower design. Additionally, the longest sections were placed at the bottom of the tower,

see Table 3.2, where the loads are dominated by axial force and bending moment. In contrast, the upper sections experience greater variation in internal stresses, justifying finer division for more precise layup optimization.

Table 3.2: Tower section division based on height and load distribution (top to bottom).

Section	Range (m)	Length (m)
S_9 (Top)	148 - 166	18
S_8	131 - 148	17
S_7	114 - 131	17
S_6	96 - 114	18
S_5	78 - 96	18
S_4	59 - 78	19
S_3	40 - 59	19
S_2	20 - 40	20
S_1 (Bottom)	0 - 20	20

From this point forward, the notation used for the different sections in this report will be $S_{i,j}$, where $i = \{1, 2, 3, 4, 5, 6, 7, 8, 9\}$ denotes the section number, and $j = \{1, 2, b\}$ indicates the concept: TC1, TC2, or the benchmark model, respectively.

3.5.1 Initial layup configuration

From the perfomed hand calculations, described in chapter 2.2.2, and the theoretical background about laminate stacking sequences, see chapter 2.2.1, the suggested initial layup configuration for all nine sections in the geometry were:

$$S_9 : [45/45/-45/-45/45/-45]_S \tag{3.1}$$
$$S_8 : [30/30/-30/-30/30/-30]_S \tag{3.2}$$
$$S_7 : [20/20/-20/-20/20/-20]_S \tag{3.3}$$
$$S_6 : [0/0/0/0/0/0]_S \tag{3.4}$$
$$S_5 : [0/0/0/0/0/0]_S \tag{3.5}$$
$$S_4 : [0/0/0/0/0/0]_S \tag{3.6}$$
$$S_3 : [0/0/0/0/0/0]_S \tag{3.7}$$
$$S_2 : [0/0/0/0/0/0]_S \tag{3.8}$$
$$S_1 : [0/0/0/0/0/0]_S \tag{3.9}$$

Generally, the hand calculations and the benchmark results, indicate that a greater number of 0° panels (increased thickness in 0° panels) is required for the bottom two-thirds of the tower, $S_1 - S_6$, to effectively withstand the axial forces and bending moments generated by both the turbine load and the increasing self-weight of the structure as height decreases. In contrast, the uppermost sections, $S_7 - S_9$, primarily experiences torsional loading, suggesting that panels with an orientation of ±45°

should be emphasized to efficiently carry the shear stresses. Additionally, fewer 0° panels are required in this region, as the self-weight is minimal at the top of the tower. Moreover, the torsional stresses become less dominant with distance from the top, which means that the initial layup for sections S_7 and S_8 does not necessarily require full ±45°-orientation. Hence, a slightly lower rotated angle was selected for these sections in the initial configuration.

3.6 Iterative optimization approach

The idea is to investigate whether there is a proposed layup configuration that optimizes the strength of the tower wall, while minimizing the thickness of the wall and thus the material consumption. To optimize the layup, an iterative approach was employed, modifying one section at a time, starting from the top section going downwards, while keeping the others constant. This approach ensured a systematic parameterization. Initially, S_9 was iterated while sections $S_1 - S_8$ remained unchanged. The results were then analyzed to determine the most optimal layup for each section individually. Subsequently, the process was repeated for S_8, keeping $S_1 - S_7$ and S_9 fixed, where the layup configuration in section S_9 corresponds to the previously optimized solution. This iterative procedure was continued systematically until all nine sections were optimized.

The iterative analysis focused on evaluating different layup configurations to determine their impact on the structural performance of the tower. Several aspects were investigated: firstly, the effect of rearranging panel order while maintaining the same orientations. Secondly, the influence of increasing or decreasing the proportion of a specific orientation within a section. Thirdly, alternative fiber orientations beyond the conventional 0° and ±45° were explored to evaluate the potential benefits of finding a sweep spot orientation. And finally, the impact of varying the thickness of certain orientations was studied to determine whether the total wall thickness could be reduced while maintaining structural performance.

To evaluate the structural integrity of the tower, both safety factors and stress distributions were analyzed for all three load cases. The analysis included both local and global strength assessments. The local analysis refers to evaluating safety factors and stress components within one section, while the global analysis refers to the verification made that no optimization has affected the safety factors in neighboring sections. Additionally, failure plots, based on maximum stress and Tsai-Hill criteria, were used to identify critical panels and guide iterative improvements.

The desired results were extracted to a *Parameter Set*, enabling small corrections directly within the set of in- and out-parameters and thereby reducing simulation time. This approach allowed systematic variation of panel orientation angles and thicknesses without manually modifying the model. Output parameters included structural responses such as total deformation, tower volume, and safety factors for the different failure criteria. Material and geometry properties were not parameterized.

4
Results & discussion

In this chapter, results obtained from the numerical analyses in ANSYS are presented and discussed. The first section focuses on the results from the iterative design of a benchmark model, followed by results from the designs of the two tower concepts (TC1 and TC2). Each section includes key insights from the iterations, highlighting the impact of different layup configurations and design choices on the tower's structural performance. These results are discussed in terms of safety factors from two different failure criteria, and the overall optimization of the tower's material usage and strength.

4.1 Benchmark model

The benchmark model consists of only 0°-oriented panels throughout the whole tower. Thus, only thickness iterations were studied for this baseline concept. The wall thickness in each section were initially 300 mm and the thicknesses were iterated for three neighbouring sections simultaneously, ($S_{9,b} - S_{7,b}$, $S_{6,b} - S_{4,b}$ and $S_{3,b} - S_{1,b}$) with a restriction, given by Modvion, that the difference in thickness between two neighbouring sections must not exceed 50 mm. In the Tables 4.1-4.2 the iterations are presented together with the local safety factors in each section.

Table 4.1: Thickness iterations and resulting safety factors for Sections 7–9 in the benchmark model under three load cases. The final selected design is highlighted.

$S_{9,b}$	$S_{8,b}$	$S_{7,b}$	Vol.	$S_{9,b}$ Max. Stress			$S_{8,b}$ Max. Stress			$S_{7,b}$ Max. Stress		
[mm]	[mm]	[mm]	[m^3]	LC1	LC2	LC3	LC1	LC2	LC3	LC1	LC2	LC3
300	300	300	1032	2.41	0.80	1.01	1.69	1.00	1.26	1.57	1.25	1.55
325	300	300	1038	2.48	0.84	1.07	1.69	1.02	1.30	1.57	1.25	1.55
325	325	300	1045	2.58	0.84	1.07	1.72	1.05	1.33	1.60	1.29	1.62
350	325	300	1052	2.65	0.88	1.13	1.72	1.08	1.37	1.60	1.29	1.62
350	325	325	1059	2.65	0.88	1.13	1.82	1.08	1.37	1.61	1.32	1.64
350	350	325	1066	2.76	0.88	1.13	1.85	1.11	1.40	1.60	1.37	1.66
375	350	325	1072	2.82	0.93	1.18	1.85	1.13	1.44	1.60	1.37	1.66
400	350	325	1079	2.88	0.97	1.24	1.85	1.14	1.46	1.60	1.37	1.66
425	375	325	1092	3.05	1.01	1.30	1.88	1.20	1.53	1.60	1.39	1.65

Section $S_{9,b}$ is the most critical section in the benchmark model, due to the heavy torsional loads. The thinnest wall thickness that can handle the torsion-dominant

load case (LC2) for the uppermost section is 425 mm. The thinnest combination of thicknesses in the top three sections is highlighted in Table 4.1, and used in further iterations for the middle- and bottom three sections, $S_{1,b} - S_{6,b}$, see Table 4.2.

Table 4.2: Thickness iterations and resulting safety factors for Sections 1–6 in the benchmark model under three load cases. The final selected design for each set is highlighted. Thickness combinations highlighted in red will fail in section $S_{2,b}$.

$S_{6,b}$ [mm]	$S_{5,b}$ [mm]	$S_{4,b}$ [mm]	Vol. [m^3]	$S_{6,b}$ Max. Stress			$S_{5,b}$ Max. Stress			$S_{4,b}$ Max. Stress		
				LC1	LC2	LC3	LC1	LC2	LC3	LC1	LC2	LC3
300	300	300	1092	1.33	1.63	1.40	1.27	1.96	1.27	1.35	2.27	1.37
275	300	300	1084	1.19	1.54	1.23	1.27	1.84	1.27	1.35	2.27	1.37
275	275	300	1074	1.22	1.54	1.29	1.17	1.85	1.20	1.26	2.13	1.28
275	275	275	1064	1.22	1.54	1.29	1.17	1.85	1.17	1.21	1.97	1.22
275	250	275	1055	1.13	1.54	1.18	1.05	1.77	1.07	1.15	1.95	1.17
275	250	250	1044	1.13	1.54	1.18	1.07	1.71	1.07	1.01	1.60	1.00

$S_{3,b}$ [mm]	$S_{2,b}$ [mm]	$S_{1,b}$ [mm]	Vol. [m^3]	$S_{3,b}$ Max. Stress			$S_{2,b}$ Max. Stress			$S_{1,b}$ Max. Stress		
				LC1	LC2	LC3	LC1	LC2	LC3	LC1	LC2	LC3
300	300	300	1044	1.09	1.80	1.10	1.14	1.87	1.15	1.17	1.80	1.15
275	300	300	1033	1.09	1.81	1.10	1.08	1.77	1.09	1.17	1.80	1.15
275	275	300	1021	1.09	1.81	1.10	1.05	1.72	1.06	1.17	1.80	1.15
275	275	275	1007	1.09	1.81	1.10	1.05	1.72	1.06	1.08	1.67	1.06
250	275	300	1009	1.03	1.69	1.04	0.99	1.62	1.00	1.17	1.80	1.15
250	275	275	996	1.03	1.69	1.04	0.99	1.62	1.00	1.08	1.67	1.06

A general observation is that the top third of the tower shows the greatest potential for improvement. Not only do the uppermost sections require relatively thick walls, but their design also influences the dimensions of the sections below them. While the upper sections increase the total material volume, this is compensated by reductions in the lower sections. Because of the larger diameters at the base, removing panels at the bottom saves significantly more volume than what is added by increasing the same amount of panels at the top. A summary of the required thicknesses section-wise is presented in Table 4.3. This highlights that varying wall thickness between segments is necessary when using unidirectional layups.

Table 4.3: Summary of the benchmark model.

Section	Layup config.	Total Thickness [mm]
$S_{9,b}$	$[0/0/0/0/0/0/0/0/\overline{0}]_S$	425
$S_{8,b}$	$[0/0/0/0/0/0/0/\overline{0}]_S$	375
$S_{7,b}$	$[0/0/0/0/0/0/\overline{0}]_S$	325
$S_{6,b}$	$[0/0/0/0/0/\overline{0}]_S$	275
$S_{5,b}$	$[0/0/0/0/0]_S$	250
$S_{4,b}$	$[0/0/0/0/0]_S$	250
$S_{3,b}$	$[0/0/0/0/0/\overline{0}]_S$	275
$S_{2,b}$	$[0/0/0/0/0/\overline{0}]_S$	275
$S_{1,b}$	$[0/0/0/0/0/\overline{0}]_S$	275

4.2 Tower Concept 1

For the first tower concept, material data for Kerto-Q was used with the possibility of arbitrary panel orientations and several panel thicknesses, as explained in chapter 2.1.1. The optimization of **TC1** was carried out with layup and thickness iterations. The layup iterations were relevant for the tower sections that require increased shear stiffness and thus twisted panels. For those parts of the tower where the torsional loads are not as dominant, only wall thicknesses were investigated.

4.2.1 Layup iteration

In this part of the result, the development of the sweet spot angle for various tower sections is shown and the optimal laminate layup based on safety factors is presented. In Figure 4.1 the sweet spot angles for the top three sections can be identified as the points where the safety factor curves for different load cases intersect. Along the x-axis, the panel orientation angle is varied, while the y-axis shows the resulting safety factor. Since the safety factor for one load case often increases at the expense of another, the intersection points represent an optimal compromise. These (sweet spot) angles are thus considered the most balanced solutions.

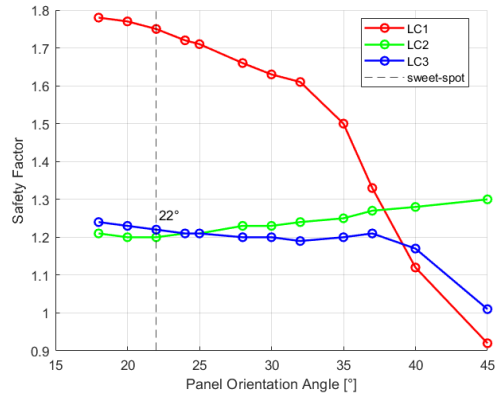

(a) $S_{9,1}$ – Maximum stress

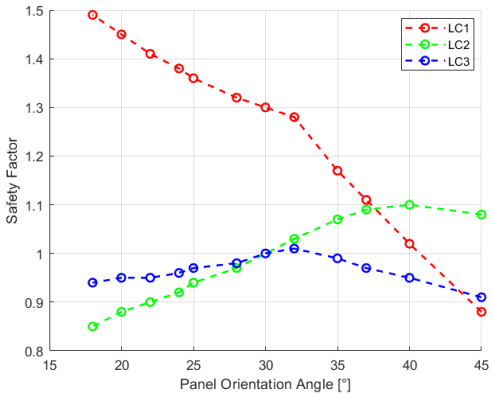

(b) $S_{9,1}$ – Tsai-Hill

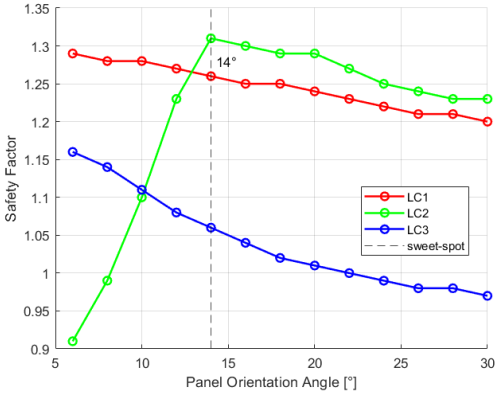

(c) $S_{8,1}$ – Maximum stress

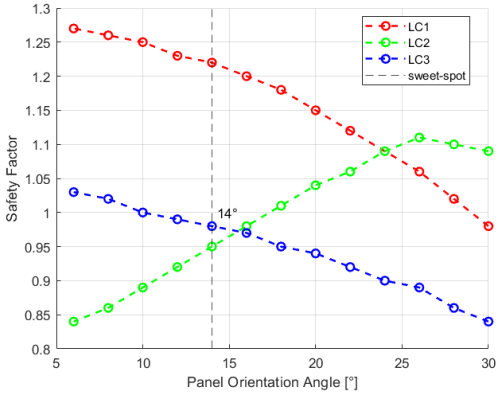

(d) $S_{8,1}$ – Tsai-Hill

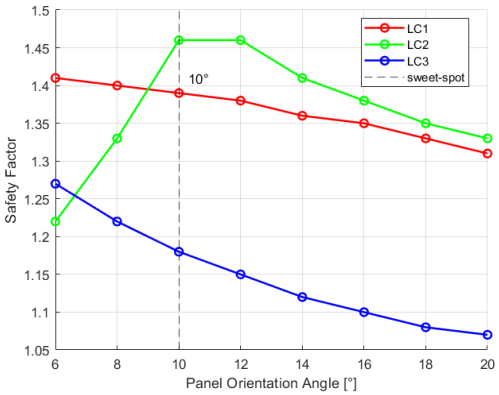

(e) $S_{7,1}$ – Maximum stress

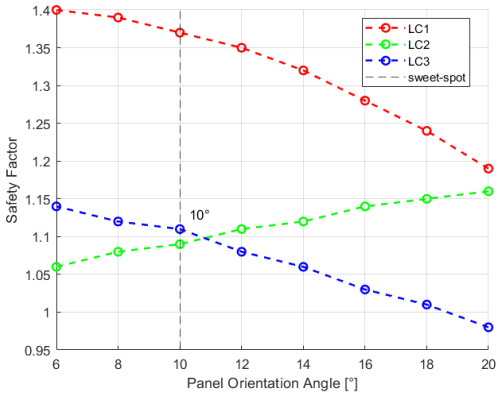

(f) $S_{7,1}$ – Tsai-Hill

Figure 4.1: Variation of local safety factors in sections $S_{9,1}$, $S_{8,1}$, and $S_{7,1}$ as a function of panel orientation for the three load cases (angle-ply laminate). The results plotted on the y-axis are based on the Maximum Stress and Tsai-Hill failure criteria.

In section $S_{9,1}$, the bending stiffness tend to decrease significantly for panel orientations larger than $\pm 35°$. The sweet spot angle for this section was found to be

22°, according to maximum stress. Observe that there is no clearly defined optimal orientation, especially in section $S_{9,1}$. Instead, the results indicate a relatively wide range of near-optimal panel orientations. In this case, angles between 18° and 27° yield similar safety factors across all three load cases. This means the sweet spot angle does not correspond to one distinct angle, but falls within a region where multiple orientations provide comparably high performance. Therefore, 22° was chosen as a representative value within this range, striking a balance between LC2 and LC3 while maintaining strong performance for LC1. This interpretive approach is applied in the evaluation of the sweet spot angles in sections $S_{8,1}$ and $S_{7,1}$, where multiple angles can be justified as optimal depending on which load case is prioritized. Worth noting in Figure 4.1b is that the intersection point between the safety factors of the two load cases does not occur at the same angle, hence the sweet spot angle will not be the same according to the Tsai-Hill criterion. The reason for this is that for angles between $15° - 45°$, the numerically derived safety factors using Tsai-Hill does not correlate equally good with the experimental safety factors. It is instead interpreted as an underestimation as it is a more conservative failure criterion. Another key observation is that the trends of the safety factor curves for LC1 and LC3 with increasing panel orientation remain similar across sections $S_{8,1}$ and $S_{7,1}$ (see Figures 4.1c-4.1f). This indicates that the increased torsional stiffness achieved at higher panel angles does not improve the overall performance under the general load case (LC3). This supports that LC3 remains primarily influenced by bending-dominated behaviour. Besides only using oriented panels throughout the wall thickness, an alternative way of balancing bending- and torsional stiffness in the top sections is to replace a pair of $\pm\theta$°-panels with 0° orientation, keeping it a balanced and symmetric layup configuration. The highlighted layup in Table 4.4 have the best balance between the safety factors for all three load cases.

Table 4.4: Numerical results for the two different failure criteria of several layup configurations in Section 9.

#	**Section 9 (sweet-spot)**	Max. Stress			Tsai-Hill		
		LC1	LC2	LC3	LC1	LC2	LC3
1.	$[45/45/-45/-45/45/-45]_S$	0.92	1.30	1.01	0.88	1.08	0.91
2.	$[22/22/-22/-22/22/-22]_S$	1.75	1.20	1.22	1.41	0.90	0.95
3.	$[45/45/-45/-45/0/0]_S$	1.22	1.21	1.32	1.14	1.00	1.21

In the same way the sweet spot angle is found for $S_{9,1}$, the optimal panel orientation for $S_{8,1}$ is shown in Figures 4.1c-4.1d. In the case of $S_{8,1}$ the sweet spot will be 14° which is an indication that the torsional load case is less dominant. Having an angle-ply laminate is not nessesarily the layup configuration that gives the best trade-off between the performance for all three load cases. In Table 4.5 the evolution of safety factors are shown, going from the initial layup configuration, via the sweet spot orientations for $S_{9,1}$ and $S_{8,1}$, to a combination of angles that provide the best balance. Layup #4 in Table 4.5 is the chosen configuration for $S_{8,1}$.

Table 4.5: Numerical results for the two different failure criteria of several layup configurations in Section 8.

#	**Section 8 (sweet-spot)**	Max. Stress			Tsai-Hill		
		LC1	LC2	LC3	LC1	LC2	LC3
1.	$[30/30/-30/-30/30/-30]_S$	1.20	1.23	0.97	0.98	1.09	0.84
2.	$[22/22/-22/-22/22/-22]_S$	1.23	1.27	1.00	1.12	1.06	0.92
3.	$[14/14/-14/-14/14/-14]_S$	1.26	1.31	1.06	1.22	0.95	0.98
4.	$[30/22/-30/-22/0/0]_S$	1.22	1.23	1.09	1.16	1.03	1.01

The optimal panel orientation for $S_{7,1}$, when having an angle-ply laminate, is 10° which can be seen in Figures 4.1e-4.1f and confirmed in Table 4.6. No other manipulations seemed as a better fit for this section of the tower.

Table 4.6: Numerical results for the two different failure criteria of several layup configurations in Section 7.

#	**Section 7 (sweet-spot)**	Max. Stress			Tsai-Hill		
		LC1	LC2	LC3	LC1	LC2	LC3
1.	$[20/20/-20/-20/20/-20]_S$	1.31	1.33	1.07	1.19	1.16	0.98
2.	$[14/14/-14/-14/14/-14]_S$	1.36	1.41	1.12	1.32	1.12	1.06
3.	$[10/10/-10/-10/10/-10]_S$	1.39	1.46	1.18	1.37	1.09	1.11
4.	$[10/10/-10/-10/0/0]_S$	1.41	1.41	1.19	1.40	1.06	1.09

With the chosen layup configurations for the top three sections (#3 in Table 4.4, #4 in Table 4.5, and #3 in Table 4.6), a safety factor distribution is obtained for the top one-third of the tower, see Figure 4.2. The grey region in all plots corresponds to the top isolated band of high safety factors, which are not of interest for the failure analysis and are therefore excluded from the discussion.

For the bending-dominated load case (LC1), the safety factor tends to decrease toward the bottom of each section, forming a U-shaped gradient profile. As we move down the tower, larger regions become influenced by this load case, consistent with the increasing effect of bending and axial forces. In contrast, Figure 4.2b illustrates the safety factor distribution under the torsion-dominated load case (LC2). Here, the minimum safety factors follow a spiral pattern through the top sections. The low safety factor regions appear to rotate slightly between sections $S_{9,1}$, $S_{8,1}$, and $S_{7,1}$, showing the torsional effects. Lastly, Figure 4.2c shows the combined load case (LC3), which reflects a mixture of the safety factor distributions from LC1 and LC2. The result is a blend of the vertical gradient from LC1 and the spiral distribution from LC2.

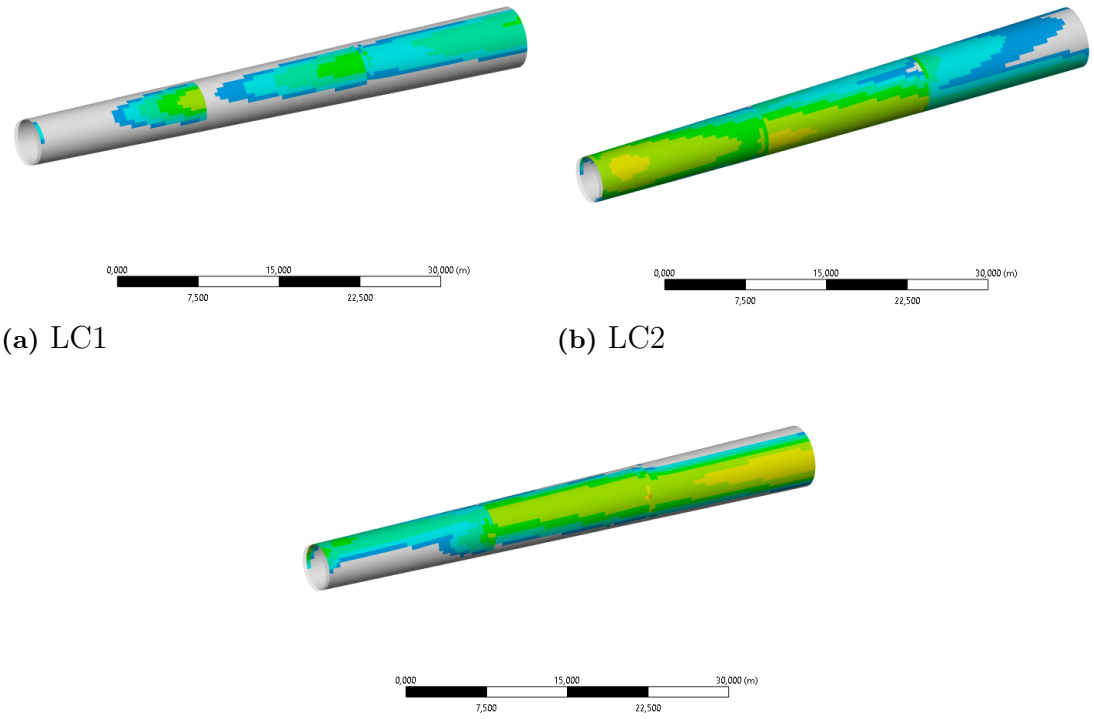

(a) LC1 **(b)** LC2

(c) LC3

Figure 4.2: Distribution of the maximum stress safety factor for all three load cases in sections $S_{7,1} - S_{9,1}$. In Figures (a)–(c), section $S_{9,1}$ is at the far left and section $S_{7,1}$ at the far right of the wall structure.

Finally, for section $S_{6,1}$ it was shown that there is no need for any oriented panels, meaning that the torsional loads will not govern the design for this region of the structure. As presented in Table 4.7, the layup configuration #6, consisting only of 0° panels yields the highest safety factor across all three load cases for both failure criteria. This indicates that introducing off-axis orientations does not improve the structural performance. Consequently, the bottom two-thirds of the tower can be considered non-critical with respect to torsional effects, and purely main grain direction, 0°, can be used in the sections $S_{1,1} - S_{6,1}$ without the need for further layup iterations.

Table 4.7: Numerical results for the two different failure criteria of several layup configurations in Section 6.

#	**Section 6 (sweet-spot)**	Max. Stress			Tsai-Hill		
		LC1	LC2	LC3	LC1	LC2	LC3
1.	$[10/10/-10/-10/10/-10]_S$	1.01	1.43	0.94	0.99	1.25	0.90
2.	$[8/8/-8/-8/8/-8]_S$	1.02	1.49	0.96	1.00	1.26	0.92
3.	$[6/6/-6/-6/6/-6]_S$	1.02	1.58	0.99	1.02	1.27	0.94
4.	$[4/4/-4/-4/4/-4]_S$	1.03	1.50	1.02	1.03	1.28	0.96
5.	$[2/2/-2/-2/2/-2]_S$	1.05	1.43	1.06	1.04	1.31	0.99
6.	$[0/0/0/0/0/0]_S$	1.06	1.41	1.11	1.05	1.35	1.02

As shown in Figure 4.3, the safety factor distribution in section $S_{6,1}$ exhibits a U-shaped profile. The minimum safety factor is found at the top of the section, i.e. at the interface with section $S_{7,1}$, and increases towards the bottom, reaching its maximum just before entering section $S_{5,1}$. This gradient suggests that the these regions of the tower are not governed by LC2. Instead, it supports the conclusion that a main grain direction (0°) is the most effective configuration for these sections, even under torsional loading.

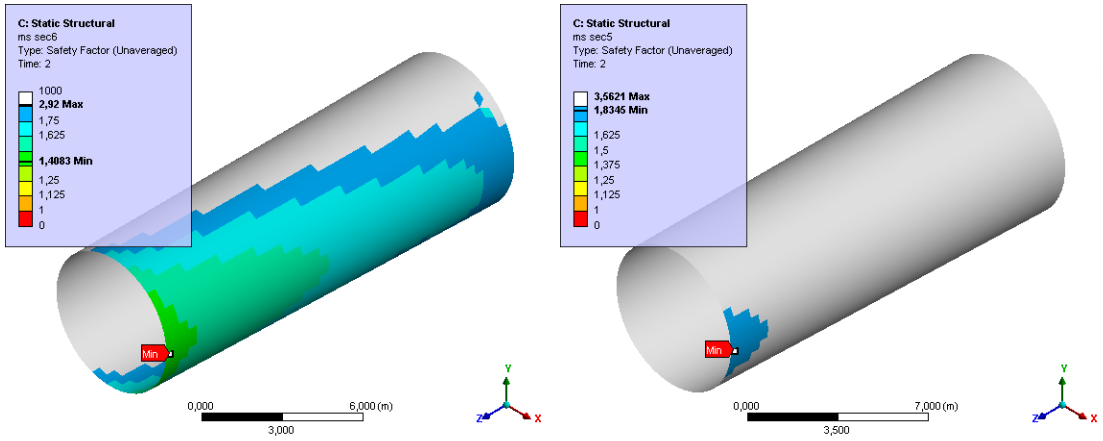

(a) $S_{6,1}$ **(b)** $S_{5,1}$

Figure 4.3: Distribution of the maximum stress safety factor for a torsion-dominant load case (LC2) in sections $S_{6,1}$ and $S_{5,1}$.

4.2.2 Thickness iteration

To minimize the wall thickness in each section of the tower, the thickness of each indivual LVL panel is parameterized and iterated. The key factor when iterating thickness is keeping the laminate balanced, i.e. the thickness for every $+\theta$ orientation has to be equal to the thickness for the corresponding $-\theta$ orientation. This is an important feature because an unbalanced laminate can lead to direction-dependent behavior. In this study, load cases include combinations of bending, axial, and torsional loads. For the torsional load case in particular, the direction of applied torque (e.g., along $+\hat{z}$) is arbitrary and could just as likely occur along $-\hat{z}$. By keeping the laminate balanced, the structural response remains symmetric and direction-independent, ensuring the results are meaningful and not biased by arbitrary load direction assumptions (see Table 3.1). For the bottom sections, $S_{1,1} - S_{6,1}$, that only have 0° panels, the thickness for an arbitrary panel is changed. Table 4.8 below illustrates how different distributions of panel thicknesses impact the performance of sections $S_{9,1}$, $S_{8,1}$, and $S_{7,1}$, having the same total wall thickness. The thickness iterations are ordered going from the top section downward. For $S_{9,1}$ and $S_{8,1}$, which include main grain direction (0°) panels in their layups, the rows are sorted to show increasing 0° panel thicknesses. This arrangement helps visualize what ratio between rotated- and non-rotated panel thicknesses that yields the most balanced performance. The notation for the arrangement of thicknesses between the panels

follow the same principle as the notation for panel orientations (as described in chapter 2.2.1), but instead of brackets, parantheses are used.

Table 4.8: Results for the local safety factors depending on thicknesses of the panels in Section 7–9.

#	**Section 9**	Total	Max. Stress			Tsai-Hill		
	[45/45/-45/-45/0/0]$_S$	[mm]	LC1	LC2	LC3	LC1	LC2	LC3
1.	$(25/25/25/25/16/16)_S$	264	0.91	1.11	1.01	0.83	0.92	0.88
2.	$(25/22/22/25/19/19)_S$	264	0.98	1.10	1.10	0.90	0.91	0.96
3.	$(22/22/22/22/22/22)_S$	264	1.05	1.08	1.18	0.98	0.89	1.04
4.	$(22/19/19/22/25/25)_S$	264	1.11	1.06	1.17	1.05	0.87	1.06
5.	$(19/19/19/19/28/28)_S$	264	1.17	1.03	1.15	1.12	0.85	1.03
	Section 8	Total	Max. Stress			Tsai-Hill		
	[30/22/-30/-22/0/0]$_S$	[mm]	LC1	LC2	LC3	LC1	LC2	LC3
6.	$(31/22/31/22/16/16)_S$	276	1.03	1.18	1.03	0.97	1.01	0.95
7.	$(25/25/25/25/19/19)_S$	276	1.06	1.17	1.04	1.00	0.99	0.96
8.	$(28/19/28/19/22/22)_S$	276	1.07	1.16	1.04	1.01	0.98	0.97
9.	$(31/16/31/16/22/22)_S$	276	1.06	1.17	1.04	1.01	0.98	0.97
10.	$(25/19/25/19/25/25)_S$	276	1.09	1.14	1.04	1.04	0.95	0.97
11.	$(28/16/28/16/25/25)_S$	276	1.08	1.14	1.04	1.03	0.96	0.97
12.	$(16/25/16/25/28/28)_S$	276	1.12	1.09	1.03	1.08	0.92	0.97
13.	$(19/22/19/22/28/28)_S$	276	1.11	1.10	1.03	1.07	0.93	0.97
	Section 7	Total	Max. Stress			Tsai-Hill		
	[10/10/-10/-10/10/-10]$_S$	[mm]	LC1	LC2	LC3	LC1	LC2	LC3
14.	$(25/25/25/25/22/22)_S$	288	1.34	1.38	1.14	1.31	1.05	1.02
15.	$(28/22/28/22/22/22)_S$	288	1.34	1.38	1.14	1.31	1.05	1.02
16.	$(28/19/28/19/25/25)_S$	288	1.33	1.38	1.14	1.30	1.04	1.02
17.	$(28/25/28/25/19/19)_S$	288	1.34	1.37	1.14	1.31	1.05	1.03

For section $S_{9,1}$, the results show that increasing the total 0° panel thickness by 12 mm leads to a significant improvement in performance for the bending-dominated load case (LC1). At the same time, the 12 mm thickness reduction in the ±45° panels does not affect the performance under the torsion-dominated case (LC2) as much. The best-performing configuration consists of 100 mm of 0° panels and 164 mm of ±45° panels, indicating that the optimal thickness ratio is approximately 40% axial (0°) and 60% rotated (±45°). For $S_{8,1}$ the results indicate that there is not much of a difference between the thickness distributions $\#6 - \#10$. However, in configurations #12 and #13, where the thickness of the more rotated (30°) panels is reduced in favor of increased thickness in the less rotated (22°) panels, a trend is observed: the safety factor for LC1 increases, while it decreases for LC2. This implies that thicker rotated panels favor torsional stiffness (LC2), whereas thicker less-rotated or non-rotated panels improve performance under axial and bending-dominated loads (LC1). Since the rotated panels are rotated to different degrees, it is not convenient to compare the ratio of thicknesses to the previous section. Finally, for $S_{7,1}$, which contains only rotated panels, the distribution of individual thicknesses has no effect

on performance, provided the total wall thickness remains constant.

When the panel thickness is modified for one section at a time, there is a risk that stress concentrations will occur due to the thickness transitions between sections. These discontinuities can lead to local failure in neighboring sections, even if their initial safety factors were approved. Therefore, the thickness of each section is not reduced below that of the section directly above it, even if the local safety factor suggests that further optimization is possible. This is done to avoid negative effects on the structural performance of the upper sections. This can be seen, for example, in section 7, where additional reductions were possible, but would have negatively affected the performance of section 8 due to the resulting thickness mismatch. For the rest of the sections ($S_{1,1} - S_{6,1}$), which consist of purely 0° orientations, thickness for an arbitrary panel in the layup was changed. The final wall thicknesses achieved are presented in Table 4.9.

Table 4.9: Results for the local safety factors depending on thicknesses of the panels in Section 1-6.

	$[\mathbf{0/0/0/0/0/0}]_S$	Total	Max. Stress			Tsai-Hill		
		[mm]	LC1	LC2	LC3	LC1	LC2	LC3
$S_{6,1}$	$(25/25/25/25/22/22)_S$	288	1.04	1.40	1.08	1.03	1.35	1.01
$S_{5,1}$	$(25/25/25/25/22/22)_S$	288	1.03	1.78	1.04	1.03	1.52	1.02
$S_{4,1}$	$(25/25/25/25/22/22)_S$	288	1.04	1.91	1.06	1.03	1.51	1.02
$S_{3,1}$	$(25/25/25/25/22/22)_S$	288	1.11	1.94	1.13	1.11	1.61	1.11
$S_{2,1}$	$(25/25/25/25/28/28)_S$	312	1.00	1.75	1.01	1.00	1.64	1.00
$S_{1,1}$	$(25/25/25/25/28/28)_S$	312	1.04	1.62	1.03	1.04	1.62	1.04

For verification, the global safety factor distribution for all three load cases are illustrated in Figure 4.4.

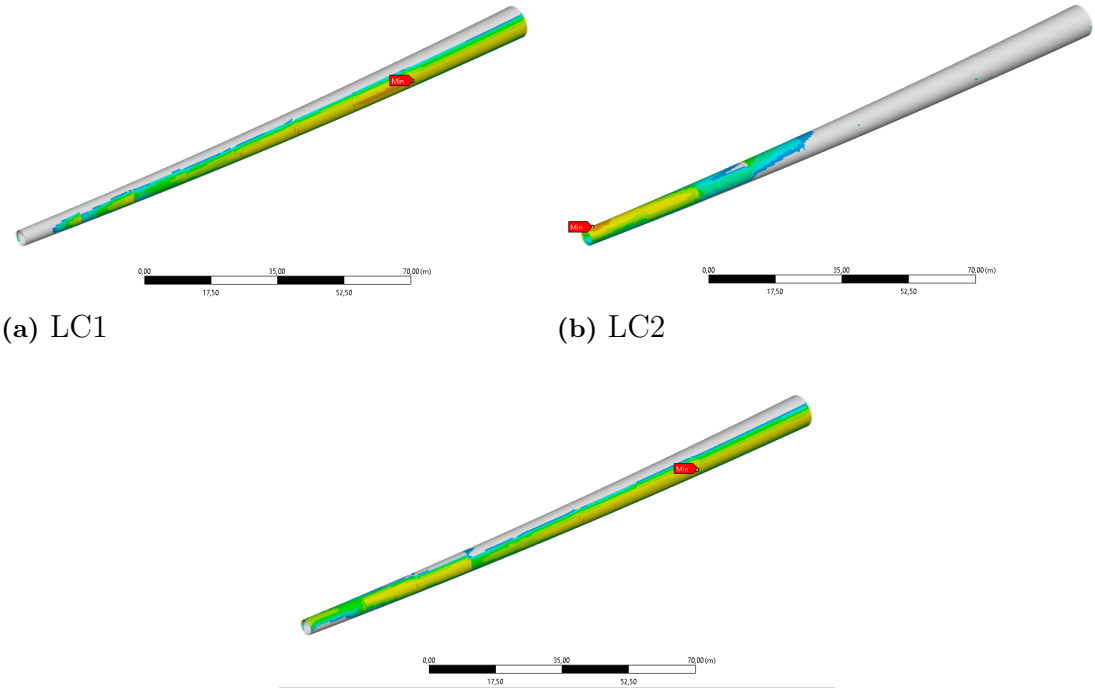

(a) LC1 **(b)** LC2

(c) LC3

Figure 4.4: Global distribution of the maximum stress safety factor for all three load cases in all tower sections.

As previously seen, the minimal safety factors occur in sections $S_{9,1}$ and $S_{2,1}$. At the top of the tower the torsinal effects (LC2) are dominating, and the safety factor minimum will therefore occur in the top section (see 4.4b). For the other two load cases (LC1 and LC3), the dominated loads are the axial force and bendning moment, which leads to the safety factor minimum found at the top of section $S_{2,1}$, indicated in Figures 4.4a and 4.4c. The total volume of the optimized TC1 was 1007 m^3 and the final design of the concept is summarized in Table 4.10.

Table 4.10: Summary of TC1

Section	Layup config.	Thickness config.	Total Thickness [mm]
$S_{9,1}$	$[45/45/-45/-45/0/0]_S$	$(22/19/19/22/25/25)_S$	264
$S_{8,1}$	$[30/22/-30/-22/0/0]_S$	$(25/19/25/19/25/25)_S$	276
$S_{7,1}$	$[10/10/-10/-10/10/-10]_S$	$(25/25/25/25/22/22)_S$	288
$S_{6,1}$	$[0/0/0/0/0/0]_S$	$(25/25/25/25/22/22)_S$	288
$S_{5,1}$	$[0/0/0/0/0/0]_S$	$(25/25/25/25/22/22)_S$	288
$S_{4,1}$	$[0/0/0/0/0/0]_S$	$(25/25/25/25/22/22)_S$	288
$S_{3,1}$	$[0/0/0/0/0/0]_S$	$(25/25/25/25/22/22)_S$	288
$S_{2,1}$	$[0/0/0/0/0/0]_S$	$(25/25/25/25/28/28)_S$	312
$S_{1,1}$	$[0/0/0/0/0/0]_S$	$(25/25/25/25/28/28)_S$	312

4.3 Tower Concept 2

Unlike the first tower concept, Tower Concept 2 uses material data for Kerto-Qe. The differences in material properties are presented in Table 2.2. Furthermore, the maximum allowable panel orientation is limited to ±25°, and only one panel thickness is available: 25 mm. The layup iterations were initially based on the sweet spot results obtained from the previous tower concept. However, due to the change in material and thereby differences in directional property ratios, the sweet spot investigation was re-simulated. The starting point was the previously identified sweet spot angles, with variations of ±4° introduced to verify whether the optimal layup orientations differ for the three upper sections in this new concept. Since only one panel thickness is available in TC2, thickness iterations can only be carried out in discrete steps by removing or adding entire panels. To enable such iterations while maintaining a balanced and symmetric laminate configuration, an even number of rotated panels is required in the layup. This ensures that thickness can be adjusted by removing or adding 0° panels.

4.3.1 Layup iteration

Since previously shown that the bottom two-thirds of the tower perform best with only 0° panels, only the top three sections were tested for different layup configurations. The sweet spot angles for TC2 are presented in Figure 4.5.

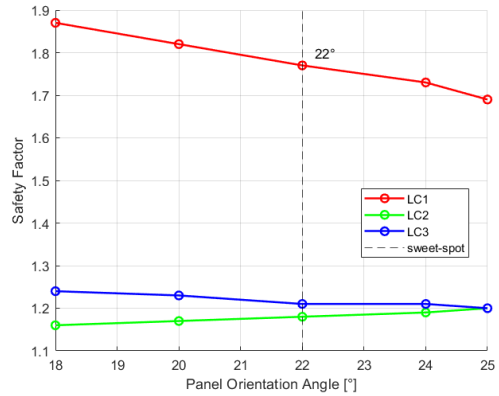

(a) $S_{9,2}$ – Max. Stress

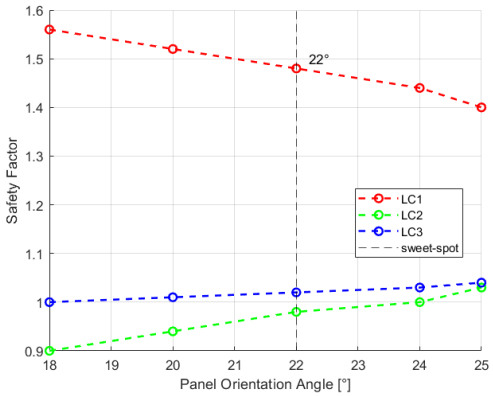

(b) $S_{9,2}$ – Tsai-Hill

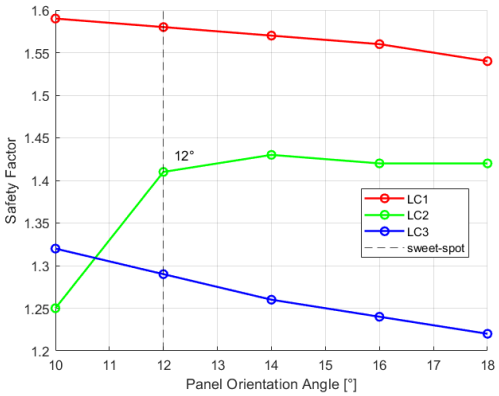

(c) $S_{8,2}$ – Max. Stress

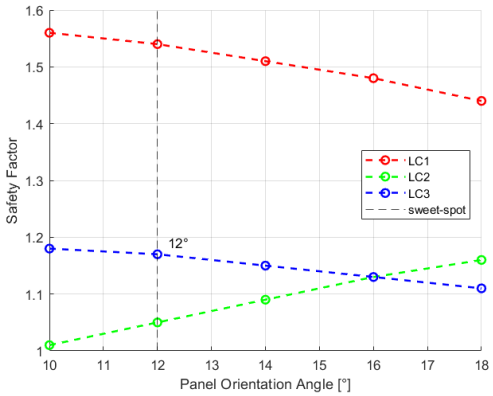

(d) $S_{8,2}$ – Tsai-Hill

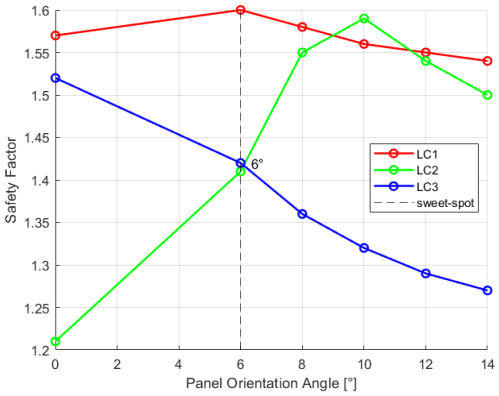

(e) $S_{7,2}$ – Max. Stress

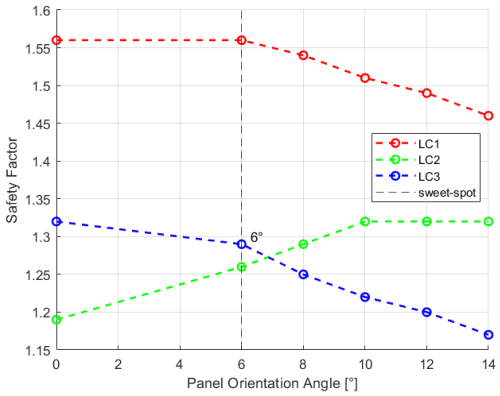

(f) $S_{7,2}$ – Tsai-Hill

Figure 4.5: Safety factor plots for two failure criteria (Maximum Stress and Tsai-Hill) for Sections $S_{9,2}$, $S_{8,2}$, and $S_{7,2}$. The optimal panel angles (sweet-spots) are found in the region where safety factors for the different load cases intersect.

Compared to the sweet spot angles obtained for Tower Concept 1 (TC1), the optimal panel orientations for the three upper sections shift slightly when the updated Kerto-Qe material data are used in Tower Concept 2 (TC2). For TC1, the identified sweet

spot angles were 22°, 14°, and 10° for sections $S_{9,1}$, $S_{8,1}$, and $S_{7,1}$, respectively. In contrast, TC2 resulted in sweet spot angles of 22°, 12°, and 6° for the same sections. Only the top section (S_9) shares the same optimal angle between the two concepts. It is important to note that the sweet spot is not always a single, well-defined value, but rather a region where multiple angles yield comparably high safety factors. As illustrated in Figure 4.5a, the top section could arguably have an optimal angle closer to 25°, yet 22° was chosen due to its more favorable performance for the first load case (LC1). Although LC2 and LC3 intersect at 25°, the variation of the safety factors are minor compared to the drop in safety factor for LC1, making 22° a reasonable choice. Moreover, in practical terms, when manufacturing panels with rotated angles, achieving an exact orientation is limited by Modvion's production tolerances. Therefore, sweet spot *regions*, where a range of angles provide similarly high safety factors, are at least as relevant as pinpointed optima. The selection of a sweet spot angle is therefore partially interpretive, as there even might exist multiple intersection points between safety factor curves for different load cases (see Figure 4.5e). The critical consideration is which load case governs the design of the section. Thus, identifying the most sensitive load case and prioritizing it in the angle selection becomes a matter of preference. In this study the chosen sweet spot angles for TC2 were 22°, 12°, and 6°, but were further changed to a layup containing an even number of rotated panels and the rest being 0°, see Table 4.11.

Table 4.11: Numerical results for the two different failure criteria of several layup configurations in Section 7–9.

#	**Section 9 (sweet-spot)**	Max. Stress			Tsai-Hill		
		LC1	LC2	LC3	LC1	LC2	LC3
1.	$[22/22/-22/-22/22/-22]_S$	1.77	1.18	1.21	1.48	0.98	1.02
2.	$[-22/-22/22/22/-22/22]_S$	1.76	1.36	1.41	1.47	0.93	1.12
3.	$[-22/-22/22/22/0/0]_S$	1.82	1.25	1.33	1.60	0.86	1.05
#	**Section 8 (sweet-spot)**	Max. Stress			Tsai-Hill		
		LC1	LC2	LC3	LC1	LC2	LC3
4.	$[12/12/-12/-12/12/-12]_S$	1.58	1.41	1.29	1.54	1.05	1.17
5.	$[-12/-12/12/12/-12/12]_S$	1.60	1.51	1.36	1.56	1.01	1.17
6.	$[-12/-12/12/12/0/0]_S$	1.62	1.44	1.34	1.59	0.96	1.13
#	**Section 7 (sweet-spot)**	Max. Stress			Tsai-Hill		
		LC1	LC2	LC3	LC1	LC2	LC3
7.	$[6/6/-6/-6/6/-6]_S$	1.60	1.41	1.42	1.56	1.26	1.29
8.	$[6/6/-6/-6/0/0]_S$	1.60	1.37	1.42	1.57	1.23	1.29
9.	$[0/0/0/0/0/0]_S$	1.57	1.21	1.52	1.56	1.19	1.32

By adding 0° panels, the safety factor for LC1—associated with bending stiffness—increases, while the torsional performance (LC2) slightly decreases. These unrotated panels enable discrete thickness iterations without losing the balanced and symmetric layup structure. As shown in Table 4.11, the highlighted layups were carried forward into the thickness iteration phase.

4.3.2 Thickness iteration

Table 4.12 illustrates how the total tower volume evolves as 0° panels are removed. For reference, a tower with a constant wall thickness of 300 mm throughout all sections would result in a total volume of 1032 m^3. Among the evaluated configurations, thickness combinations that are highlighted in red indicate failure, while the thickness combinations highlighted in green are the chosen wall thicknesses. Here, $S_{2,2}$ becomes the critical section, with safety factors dropping to exactly 1.00 in both LC1 and LC3. The safety factor distribution for all three load cases are illustrated in Figure 4.6.

Table 4.12: Comparison of safety factors and tower volume during progressive thickness reduction from the initial 300 mm configuration.

$S_{9,2}$	$S_{8,2}$	$S_{7,2}$	Vol.	$S_{9,9}$ Max. Stress			$S_{8,9}$ Max. Stress			$S_{7,9}$ Max. Stress		
[mm]	[mm]	[mm]	[m^3]	LC1	LC2	LC3	LC1	LC2	LC3	LC1	LC2	LC3
225	225	225	970	1.25	1.20	1.10	1.20	1.13	1.14	1.11	1.29	1.17
200	225	225	964	1.25	1.14	1.09	1.20	1.13	1.14	1.11	1.29	1.17
200	200	225	957	1.27	1.03	1.06	1.06	1.12	1.03	1.11	1.06	1.10
200	200	200	950	1.12	1.12	1.00	0.96	1.06	0.97	1.07	1.21	1.12
$S_{6,2}$	$S_{5,2}$	$S_{4,2}$	Vol.	$S_{6,9}$ Max. Stress			$S_{5,9}$ Max. Stress			$S_{4,9}$ Max. Stress		
[mm]	[mm]	[mm]	[m^3]	LC1	LC2	LC3	LC1	LC2	LC3	LC1	LC2	LC3
250	250	250	901	1.11	1.29	1.17	1.07	1.73	1.08	1.15	1.95	1.17
225	250	250	893	0.94	1.28	0.97	1.07	1.61	1.08	1.15	1.95	1.17
225	225	250	884	1.01	1.28	1.06	0.94	1.59	0.96	1.05	1.78	1.07
225	225	225	873	1.01	1.28	1.06	0.97	1.57	0.97	0.98	1.61	0.99
$S_{3,2}$	$S_{2,2}$	$S_{1,2}$	Vol.	$S_{3,9}$ Max. Stress			$S_{2,9}$ Max. Stress			$S_{1,9}$ Max. Stress		
[mm]	[mm]	[mm]	[m^3]	LC1	LC2	LC3	LC1	LC2	LC3	LC1	LC2	LC3
250	275	275	852	1.04	1.71	1.05	1.00	1.64	1.00	1.08	1.68	1.07
250	250	275	839	1.09	1.82	1.10	0.96	1.58	0.97	1.08	1.68	1.07

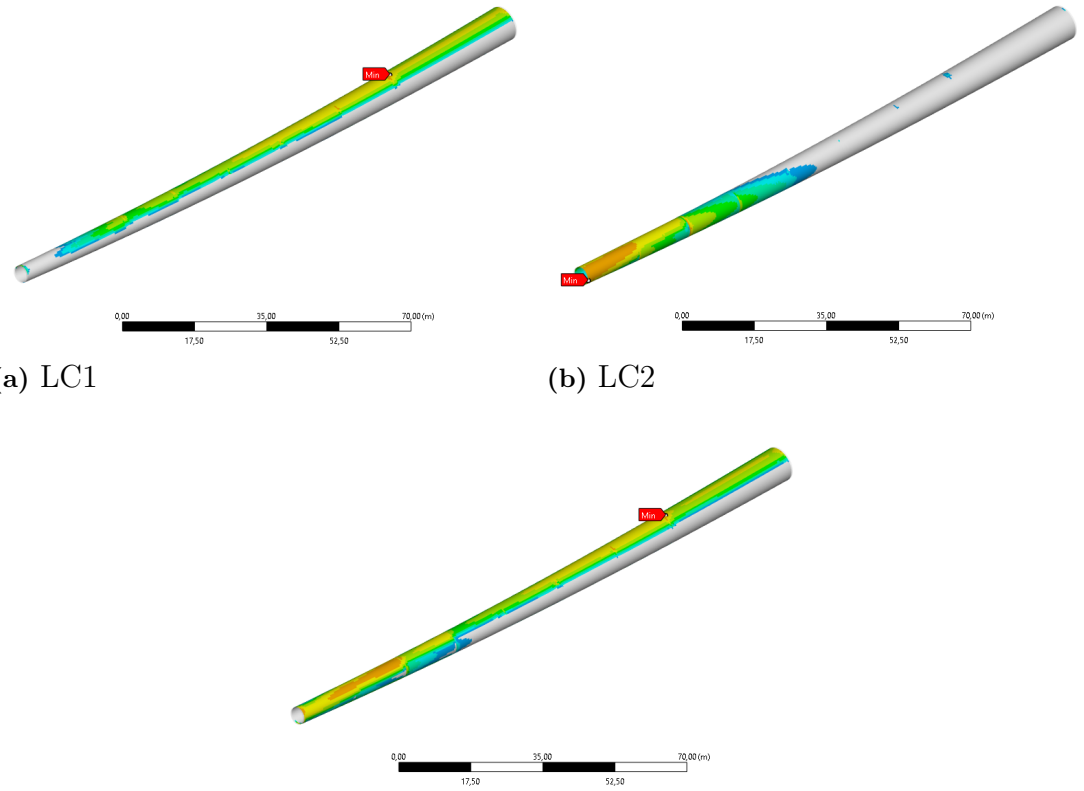

(a) LC1 **(b)** LC2

(c) LC3

Figure 4.6: Global distribution of the maximum stress safety factor for all three load cases in all tower sections (TC2).

As for the first tower concept, TC2 will also have its safety factor minima in sections $S_{2,2}$ and $S_{9,2}$. The grey region in the color plots corresponds to the top isolated band of high safety factors, which are not of interest for failure analysis and therefore not discussed further. The final design for TC2, summarized in Table 4.13, results in a total tower volume of 852 m^3.

Table 4.13: Final layup and thickness configurations for all sections in Tower Concept 2 (TC2).

Section	Layup config.	Thickness config.	Total Thickness [mm]
$S_{9,2}$	$[-22/-22/22/22]_S$	$(25/25/25/25)_S$	200
$S_{8,2}$	$[-12/-12/12/12]_S$	$(25/25/25/25)_S$	200
$S_{7,2}$	$[6/6/-6/-6/\overline{0}]_S$	$(25/25/25/25/\overline{25})_S$	225
$S_{6,2}$	$[0/0/0/0/0]_S$	$(25/25/25/25/25)_S$	250
$S_{5,2}$	$[0/0/0/0/0]_S$	$(25/25/25/25/25)_S$	250
$S_{4,2}$	$[0/0/0/0/0]_S$	$(25/25/25/25/25)_S$	250
$S_{3,2}$	$[0/0/0/0/0]_S$	$(25/25/25/25/25)_S$	250
$S_{2,2}$	$[0/0/0/0/0/\overline{0}]_S$	$(25/25/25/25/25/\overline{25})_S$	275
$S_{1,2}$	$[0/0/0/0/0/\overline{0}]_S$	$(25/25/25/25/25/\overline{25})_S$	275

5
Conclusion

This study sets out to investigate the potential for material optimization in a laminated timber tower structure through adjustments in wall layup and thickness configuration. The aim is to evaluate how different design strategies, represented by different tower concepts, can reduce material usage while ensuring structural safety under three different load cases.

As shown in Table 5.1, the final optimized design (TC2) achieved a significant material reduction of 15.4% compared to the benchmark model. While TC1 maintained the same total volume as the benchmark, it demonstrated how a slight change in material data (Kerto-Q and Kerto-Qe) can influence the distribution of wall thickness across sections. Table 5.1 also provides information about the thickness for the thickest and thinnest tower wall sections for all three designs.

Table 5.1: Material optimization

Model name	**Volume** $[m^3]$	**Percentage**	**Thickest [mm]**	**Thinnest [mm]**
Benchmark	1007	100%	425	250
TC1	1007	100%	312	264
TC2	852	84.6%	275	200

The biggest difference between the benchmark model and the tower concepts (TC1 and TC2) is the location of the thickest section. In the benchmark model, the top section requires the thickest tower wall, whereas in TC1 and TC2, the thickest sections are instead located at the bottom of the tower, with the top being the thinnest. This reversal is due to the change in panel orientation at the top of the tower in TC1 and TC2, which is specifically designed to better resist the torsional effects induced by the turbine. It was also shown that the lower two thirds of the tower do not benefit from rotated panels and perform best with purely 0° orientations. In contrast, the upper three sections all have an optimal panel orientation, also called the *sweet-spot* orientation. The sweet spot angle gradually increases going from the bottom to the top of the tower, indicating the dominance of the torsional loads at the top of the tower. In some sections, more than one sweet spot angle may exist, or there may be a range of angles that yield comparable safety factors. In such cases, the final choice becomes a matter of design preference, depending on which load case is prioritized in that specific region.

However, while these results provide valuable insight, they are shaped by the model-

ing choices and simplifications made throughout the study. Certain limitations and assumptions may have influenced the outcome — and recognizing them is essential for understanding both the strengths and the boundaries of the conclusions drawn. One such limitation is the division of the tower into nine sections. In particular, the upper sections, where torsional loads are more significant and the panel orientation is more sensitive, could potentially benefit from a finer subdivision. By dividing these top sections into smaller segments, the sweet spot angle could be adjusted more gradually along the height of the tower. On the other hand, the choice of nine sections is justified by real-world logistics, and since the lower segments are governed primarily by axial forces and bending moments, they do not require varied layup configurations — making larger segments at the base a reasonable design choice. Another choice that most probably have influenced the outcome of this study is the load cases. Two out of the three load cases chosen in the study represent extreme scenarios for the different types of loads. The bending moment and torsional loads are isolated to evaluate how the panel orientations respond to each load type individually, while a more general load case (LC3) includes all load types and serves as a verification case. However, the number of load case combinations is significantly greater and there is possibly a load case that would have caused the safety factor in a certain section to be < 1. Buckling and delamination are also not something that this study provides an answer to. Regarding buckling, it can be said that there is global and local buckling, where the global refers to the entire tower, while the local refers to the buckling of a single section. The local type of buckling involves a delamination in the tower wall in the section, which is something that needs to be investigated further. It is something that is affected by the adhesive and its properties. The fact that it is not taken into account in this study is because the classical laminate theory used has the limitation that it assumes perfect lamination and no stresses out of plane, i.e. in the radial direction in this case.

5.1 Future perspectives

One key observation from this study is the impact that a small improvement in longitudinal strength can have on material optimization. By comparing the two tower concepts TC1 and TC2—where the only difference is the material data used (Kerto-Q vs. Kerto-Qe)—it becomes evident that an increase in compressive and tensile strength leads to a reduction in total material volume. This highlights how sensitive the final design is to improvements in the mechanical properties of the material, especially the longitudinal direction. The strength data used for Kerto-Qe in this study is based on modified values derived from material testing. This suggests that if future updates or variations in the DoP (Declaration of Performance) confirm even higher strength values, particularly in the longitudinal direction, it could further improve the potential for material-efficient design. Continued material development and validation through testing should therefore be seen as one key for future improvements.

Another suggestion for future investigations, from a material optimization perspective, is to explore alternative reinforcement solutions that complement LVL struc-

tures. The key is to identify composite materials that can be effectively integrated into the existing manufacturing process involving glued LVL panels. For instance, the bottom sections of the tower could be reinforced in the longitudinal direction using a fiberglass composite sheet, either embedded between the LVL layers or applied externally to the wall. Alternatively, reinforcement could be focused on the upper sections, where a new sweet spot orientation for the reinforcement is used, allowing the LVL panels to remain purely in the 0° direction. This kind of hybrid approach might be a solution in the future that not only provides improved strength and structure in the tower wall, but also offers a cost-effective solution.

Bibliography

[1] A. Quilligan, A. O'Connor, och V. Pakrashi, "Fragility analysis of steel and concrete wind turbine towers," *Engineering structures*, vol. 36, ss. 270–282, 2012.

[2] B. P. Gilbert, H. Bailleres, H. Zhang, och R. L. McGavin, "Strength modelling of laminated veneer lumber (lvl) beams," *Construction and Building Materials*, vol. 149, ss. 763–777, 2017.

[3] Forest Machine Magazine, "Modvion's first commercial wooden wind turbine tower," Feb. 2024. Accessed: 2025-05-09.

[4] A. Romero och C. Odenbreit, "Experimental investigation on strength and stiffness properties of laminated veneer lumber (lvl)," *Materials*, vol. 16, nr. 22, s. 7194, 2023.

[5] N. Stark och Z. Cai, "Wood-based composite materials: panel products, glued laminated timber, structural composite lumber, and wood–nonwood composites," *Chapter 11 in FPL-GTR-282*, ss. 11–1, 2021.

[6] Federation of the Finnish Woodworking Industries, *European LVL Handbook*. Federation of the Finnish Woodworking Industries, 2019.

[7] M. Ardalany, M. Fragiacomo, P. Moss, och B. Deam, "An analytical model for design of reinforcement around holes in laminated veneer lumber (lvl) beams," *Materials and structures*, vol. 46, ss. 1811–1831, 2013.

[8] M. Dedijer, S. N. Roche, och Y. Weinand, "Shear resistance and failure modes of edgewise multiple tab-and-slot joint (mtsj) connection with dovetail design for thin lvl spruce plywood kerto-q panels," in *World conference on timber engineering*, 2016.

[9] B. D. Agarwal, L. J. Broutman, och K. Chandrashekhara, *Analysis and Performance of Fiber Composites*. Wiley, 4 uppl., 2017.

[10] Composite Materials Hub, "Classic laminate theory," 2023. Accessed: 2025-05-07.

[11] N. T. Mascia och R. A. Simoni, "Analysis of failure criteria applied to wood," *Engineering Failure Analysis*, vol. 35, ss. 703–712, 2013.

[12] S.-C. Oh, "Applying failure criteria to the strength evaluation of 3-ply laminated veneer lumber according to grain direction by uniaxial tension test," *Construction and Building Materials*, vol. 25, nr. 3, ss. 1480–1484, 2011.

[13] M. Merhar, "Application of failure criteria on plywood under bending," *Polymers*, vol. 13, nr. 24, s. 4449, 2021.

[14] European Committee for Standardization, *EN 1990:2002 Eurocode – Basis of Structural Design*. Brussels: CEN, 2002. Annex A1, Table A1.1.

DEPARTMENT OF SOME SUBJECT OR TECHNOLOGY
CHALMERS UNIVERSITY OF TECHNOLOGY
Gothenburg, Sweden
www.chalmers.se

CHALMERS
UNIVERSITY OF TECHNOLOGY